Development and calibration of a model for the dynamic simulation of fans with induction motors

Massimo Vaccarini[a], Alessandro Carbonari[1a], Miquel Casals[b]

[a] *Universitá Politecnica delle Marche, Department of Civil and Building Engineering and Architecture, via Brecce Bianche 12, 60131, Ancona, Italy*
[b] *Universitat Politecnica de Catalunya, Department of Project and Construction Engineering, Group of Construction Research and Innovation, C/Colom 11, 08222 Terrassa, Spain*

Abstract

In this paper a model for the dynamic simulation of fans used in mechanical air supply systems is described. Thanks to this model, the behavior of fans subject to control by variable frequency drives (VFD) can be predicted, which includes power absorbed by the fan and expected ventilation rates. Hence, it can help design energy control systems for buildings. The proposed model was based on the Modelica language and was developed from the dynamic phasor domain representation, because this representation is a trade-off between the basic non transient representation, that is computationally efficient but cannot describe fan dynamics, and the dynamic time domain model, that is the most representative one but computationally very demanding. A comparison among these models showed that, within fan frequency variations typical of ventilation systems in buildings, the phasor domain model is as representative as the more complex dynamic time domain model in terms of prediction of the dynamic behavior, that is neglected

by the basic non transient model. Moreover, the new phasor domain model was validated against measured data relative to a fan installed in a subway station in Barcelona. Thanks to this model, energy consumption of dynamically driven fans can be estimated at the simulation stage, at the expense of a reasonable computational effort.
Keywords: facility operation and control, fans, induction motors, VFD, dynamic simulation

---

1. Introduction

Due to the huge amount of energy consumption determined by buildings, HVAC renovation of the existing building stock can provide a rather high contribution to the overall energy saving. Renovation often consists in the partial replacement of aged components and in the definition of new control strategies. However, the design and development of advanced control strategies, whose performances are usually affected by several parameters, requires testing of alternative strategies, either in the field or through simulation, prior to implementation (Chen and Treado (2014)). Indeed, the availability of reliable models would allow designers to compare and evaluate control strategies at the design phase. The models should be used first to establish the baseline and then to predict expected performances by candidate control strategies, as a result of enhanced regulation and control of HVAC, in order to select the best one. Moreover, simulation models should be used not only to select the best control strategy, but also to accurately estimate expected

savings and include such figures in cost-benefit analyses.

Several reasons are produced in literature to stress the importance of user friendly simulators. First, designers should be allowed to easily change parameters and immediately evaluate results, as explained in Tomažič et al. (2013). Even Nagano et al. (2006) showed at what extent user-friendly design and performance prediction tools can help in the execution of quick feasibility studies. Several authors highlighted that simulators should be able to carry out reliable simulations in short times, e.g. in Park and Krarti (2015). Otherwise, designers would be hindered in the process of evaluating candidate control solutions, before making a final decision, due to the rather high computational effort. In addition, the availability of fast and reliable simulation models is critical when they are integrated in real-time control systems. In this case, a controller exploits a simulation unit in order to evaluate how the system would evolve within each of any candidate and alternative control strategies. Considering that the controller must accomplish each control step in short time (usually in the order of minutes) and that a huge number of iterations are performed in each control step, the simulation effort required to run the model is bound to be very limited. Basically, dynamic models enable researchers to test new control concepts and to optimize the simulated system's behavior under unsteady boundary conditions, that would not be feasible with the use of just a steady state approach (Starkloff et al. (2015)). Dynamic models were critical even in the process of evaluating potential faults in advance, such as in preventive maintenance of rooftop

units: a baseline model of variable frequency driven compressors installed on rooftop units was setup, then deviations from expected behavior could be assessed to implement automated fault diagnosis (Li et al. (2015)).

The work reported in this paper was targeted to find a trade-off for modeling induction motor fans, so as it could be both accurate enough for energy saving estimation and computationally efficient at the same time.

Induction motor fans are typically used in air supply systems of buildings and they are responsible for relevant power consumption. For example, in the test-case considered in this paper, that is relative to the ventilation system of a metro station, two fans are in operation for fifteen hours per day in weekdays and twenty-one hours per day in weekends. Hence, there is a great potential for energy savings, but an accurate evaluation of achievable results can be attained just in case a dynamic model is set up for simulations. The model described in this paper was based on the Modelica language, because Modelica was specifically developed for the simulation of control systems integrated in multi-physics domains, as explained in Wetter (2009a). Modelica based models can take into account several physical phenomena, such as heat and mass transfer and fluid-dynamics. For that reason, the model developed in this paper was expanded from the Modelica `Buildings` library and was developed in the Dymola programming environment, and it was made compliant with models relative to building components and HVAC systems. In fact, the current version of the Modelica `Buildings` library used for the application described in this paper offers components that can be

used to develop two different types of induction motor models: the first one exploits the basic stationary representation, whereas the second one exploits the time domain representation. The former is computationally very efficient but is not able to simulate the dynamics of fan induction motors; the latter is very accurate and exposes every parameter of fan induction motors, but is computationally very demanding.

Considering the premises described above, the main contributions provided by this paper are:

- a component extended from the Modelica `Buildings` library was built, which was based on the phasor representation of induction motors, so as to be able to account for the dynamic behavior of induction motor fans, while requiring limited computational effort for simulation;
- calibration and validation of the aforementioned component against measured energy consumption;
- a comparison between the power consumption figures estimated under transient conditions by a fan model based on the phasor representation and the figures estimated by both the basic stationary and time domain representations, that are already available in the current Modelica library.

The validation took advantage of data measured during the operation of a real fan equipped with induction motors and installed in the "Passeig de Gràcia" metro station in Barcelona, which is a fan driven by Variable Frequency

Drives (VFD), hence its rate can be adjusted according to actual ventilation needs in the station. The comparison between the model developed in this paper and the other two models was targeted to two main goals:

- assessing at what extent the phasor representation model is more accurate than the basic stationary one and less accurate than the the domain representation;
- estimating how much more accurate the phasor representation model is than the basic stationary representation, while the fan is dynamically driven (i.e. transient behavior) over a typical day it is in operation.

In the next Section no. 2 the relevant state of the art is analyzed, along with some further remarks about the steps ahead provided by the work described in this paper. The following Section no. 3 is split into two more subsections: sub-section 3.1 describes the proposed Modelica component as it was developed by means of the Dymola environment, whereas sub-section 3.2 reports on the related analytics. Section no. 4 was split into two subsections. The first one (no. 4.1) includes a description of the fan with induction motor used for calibration and of the metro station where the fan was installed. The second one (no. 4.2) includes a description of the experimental dataset collected while the fan was in operation, in order to calibrate the simulation model and shows that an opportune tuning of some parameters made available by the model gives back a very good matching between simulation results and measured power plots. Then, the performances of the

model were compared with the basic stationary and the time domain representation models, whose development is the subject of sub-section no. 5.1 and whose dynamic behavior was assessed in sub-section no. 5.2. Finally, conclusions are discussed in section no. 6.

2. Scientific background

2.1. Simulation of integrated systems

As stated by Kral et al. (2009), partial load efficiency of induction motors should be computed for the determination of the nominal operating point when subjected to electric drives. Although fans and pumps are designed to perform during peak loads, these loads occur rarely during the operating year. Therefore, in order to control flow during off-max load conditions, VFDs are often used to deliver only the required flow while reducing energy consumption. A good estimation of energy saving deriving from such a control policy is well described by the so called affinity laws (Wildi (2002)): when the air flow rate generated by fans is reduced by means of a rotational speed reduction, the corresponding decrease in absorbed power will follow a cubic mathematical relationship. However, the dynamic behavior of induction motors cannot be represented by means of affinity laws, and more refined simulation tools and mathematical models are needed. Once those models are available, they can be exploited for prediction of potential savings that can derive from energy improvement actions to be implemented in buildings.

Designers of integrated control systems for existing buildings usually develop a model relating to the current scenario of the buildings as a first step; then, a calibration methodology is applied to assure accuracy; finally, several opportunities for energy saving supplied by renovation actions and enhanced control systems are assessed based on the same calibrated model (Raftery et al. (2011)). In conclusion, whenever enhanced control systems integrated in existing large buildings must be simulated, the use of accurate dynamic simulation tools is mandatory.

The range of products presently available for building performance simulation spans from spread-sheet to more advanced special-purpose simulation tool (complexity-wise), and from tools that handle a single aspect of the building design, to tools that integrate multiple aspects of the building design (integration-wise), as detailed in Trčka and Hensen (2010). As for applications relative to advanced HVAC control, process controllers are usually adopted, which adjust the control variables to meet the required set point in spite of disturbances and considering the system dynamic characteristics. Still more advanced are supervisory controllers, that are high level controllers allowing complete consideration of the system level characteristics and interactions among all components and their associated variables. From a modeling point of view, controllers are represented by equations that must be satisfied in every simulation step. The controllers direct the interaction between building and system, as well as interactions between components within the system. Possibilities to simulate different advanced controllers in

state-of-the-art building performance simulation tools are limited (Trčka and Hensen (2010)). Some tools offer pre-defined control strategies (i.e. system-based simulation tools), some offer flexibility in specifying only supervisory controllers (e.g. EnergyPlus) and some even in specifying local controllers (TRNSYS, ESP-r). The domain-independent environments, such as MATLAB and Modelica/Dymola, are efficient tools for designing and testing of controllers in a simulation setting, but need that models of all other physical phenomena are developed within libraries (Trčka and Hensen (2010)).

In order to contribute in this field, a Modelica-based model for the transient simulation of fans with induction motors is proposed in this paper, which can facilitate the dynamic simulation of buildings equipped with such systems driven by VFD. Indeed, many authors have worked on similar topics. A coupling program with a text-mode interface between building simulation and computational fluid dynamics simulation was developed for thermal prediction relative to naturally ventilated indoor environments (Wang and Wong (2008)). More specifically, ESP-r and Fluent tools were used for simulating heat transfer and fluid dynamics, respectively. Again, an ad-hoc numerical algorithm was implemented in TRYNSIS in order to predict the energy performance of a hybrid solar air conditioning system under transient loads (Ha and Vakiloroaya (2015)). In the same TRYNSIS software platform two hybrid micro-generation systems in a load sharing application among residential and office buildings were successfully modeled by Canelli et al. (2015). Another customized model was developed to simulate the performance of a controller

designed for keeping exhaust level inside a highway tunnel within acceptable limits by means of primary ventilation control (Ferkl and Meinsma (2007)).

The correct design of the control system is very often necessary to attain both improved comfort for users and increased energy performance, like in the case described by Aghemo et al. (2014), where a management system was used to set up a customized control in a ten-office building, that exploited a distributed intelligence system to optimize the behavior of lighting and cooling systems. The authors pointed out that a correct design is absolutely necessary for satisfaction of users and maximization of performances, hence the need for a reliable simulation tool can be inferred.

2.2. The Modelica language

A number of studies were focused on the Modelica/Dymola environment, that was shown, by means of comparative studies, to be reliable enough, e.g. to provide a simulation tool for testing advanced control solutions to be integrated in chilled water systems (Ali et al. (2013)). The Modelica/Dymola simulation tool can manage to simulate highly integrated and complex energy and control systems, even because a number of libraries are available within the Modelica package, that can be extended beyond the use envisaged by developers (Wetter (2011)). Furthermore, Modelica/Dymola is able to face the specific requirements posed by buildings, that may be classified as heterogeneous systems, because they involve multiple domains, including thermodynamics, fluid dynamics, heat and mass transfer, electrical systems,

control and communication systems. They also involve multiple temporal and spatial scales, and their evolution can be described by coupled differential equations, discrete equations and events, as detailed in Wetter (2011).

There is evidence that Modelica performs more than satisfactory even in complex domains. In one case in which a French railway station building was modeled and its thermal and electrical loads estimated, the validation deviations were below 10% (Traore et al. (2013)). The same tool was suitable for accurately modeling single components of building equipment, such as a dynamic coil in the air handling units, which was able to predict the cooling performance when subjected to changeable boundary conditions (Li et al. (2009)).

The execution of a Modelica model also performs automatic differentiation followed by the generation and compilation of a C/C++ code (Ali et al. (2013)).

Among the main positive features provided by this modeling environment, the following ones have been highlighted in relevant literature: acausal, declarative modeling; code transparency; encapsulation and modularity; inheritance and reusability. Equation-based languages allow any model developer to declare a set of algebric equations, ordinary differential equations, and finite state machines, that define the physics of a component or the logic of a control sequence. These equations do not need to be explicitly ordered. A model translator analyzes, rearranges and solves them symbolically, as far as possible, using computer algebra to reduce the number of variables that

need to be solved during the time integration. Subsequently, an executable code is generated and linked to numerical solvers. More details can be found in Cellier and Kofman (2006). In addition, the thermal simulation of buildings is facilitated by the support of a library, the so called `Buildings` library, that has been developed and is still being revised and subject to versioning (Wetter (2009b)). Moreover, the Buildings library is still being extended and is subject to improvements, not only introduced by its developers but also by users. It is open source and allows rapid prototyping of new buildings, analysis of the operation of existing buildings, development and assessment of building control algorithms, reuse of models during operation for energy minimizing controls, fault detection and diagnostics.

In view of the aforementioned capabilities of the Modelica modeling language in the integrated simulation of energy and control systems, this paper presents a phasor representation model for the dynamic simulation of induction motor fans, which was extended from the `Buildings` library and which can be re-used in any Modelica based model.

3. The phasor representation model

3.1. The new Modelica/Dymola component (DP-model)

The induction motor fan model was developed in the Dymola environment based on Modelica and on the `Buildings` library by using the dynamic phasor representation (*DP-model*) of the electric motor. The dynamic phasor model described in this paper was extended from the `Buildings` v1.3 library,

because this is the library on which the model of the metro station used in the calibration and validation in sub-section 4.1 was based. However, it is straightforward to use it also with any newer available version. The comparison between this model and other two alternative representations, i.e. the basic stationary model and the dynamic time domain model, will be provided in sub-section 5.1.

The induction motor fan model is based on the following structure (please check Figure 1), on which every mentioned component was labelled with numbers. The model is made up of the following main components:

1. one inlet fan duct that takes air from the outside;
2. one outlet fan duct that conveys the air onto the platform;
3. one valve that stops air flow when the fan is switched-off;
4. one alternative air flow path that models leakage losses;
5. two air columns that model the altitude difference between the fan inlet and outlet;
6. one axial impeller;
7. one bi-directional electric motor that spins the impeller;
8. one inverter that drives the motor through a frequency input and returns the absorbed active power;
9. one air flow sensor that measures air flow entering the fan inlet (`port_a`).
10. one I/O data bus.

In order to implement the dynamics of the electric motor, the impeller model has been extracted from the Buildings library and is represented as

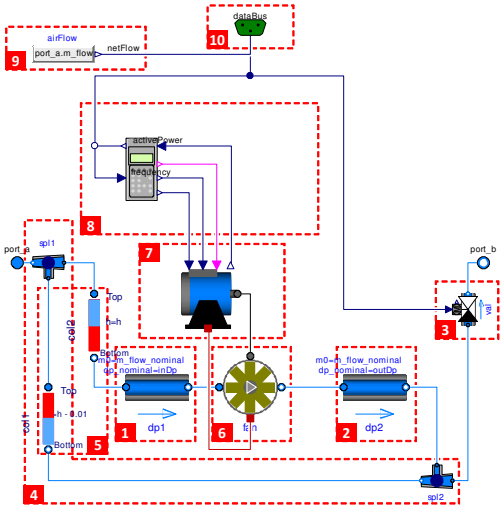

Figure 1: The phasor representation model (DP-model) developed in Dymola environment: (1)/(2) inlet/outlet fan ducts, (3) valve, (4) leakage, (5) air columns, (6) axial impeller, (7) electric motor, (8) inverter, (9) air flow sensor, (10) I/O data bus.

component (6) in the DP-model. This model derives from the idea that information about sinusoidal signals involved in motor functioning is not explicitly needed when simulating the energy consumption of buildings, and that intervals for ventilation control are usually much longer than power supply periods. These considerations allow designers to assume as valid the hypothesis of steady-state sinusoidal signals, hence the motor can be modeled by means of a phasor representation. Therefore, a new model for the three-phase asynchronous induction motor (7) was developed and included in the DP-model together with a new inverter model (8) that establishes the relationship between voltage and frequency applied to the motor and reads the active absorbed power as output. All the details about the corresponding analytics will be provided in sub-section 3.2.

3.2. Physics of the phasor representation model

The input frequency f, coming from the controller, is fed to the DP-model through the dataBus depicted at the top of Figure 1 (i.e. component no. 10). This value is forwarded to the inverter and to the valve. The inverter computes the voltage V to be applied to the motor according to:

$$V = \left| \frac{nominalVoltage}{nominalFrequency} \cdot f \right| \tag{1}$$

The inverter receives as input the active power absorbed by the motor to which it adds its own power consumption, based on pre-set efficiency parameters, prior to forwarding it to the `dataBus`. The three-phase Asynchronous Induction Machine (AIM) is then fed by the given frequency (`RealInput f`), voltage (`RealInput V`) and by a Y/Δ selection flag. Considering that the fan motor is driven by an inverter, a Y connection was used. The motor shaft spins the impeller, represented as the `fan` component close to the bottom of Figure 1. The impeller model, as stated above, is a direct extrapolation of the class named `FlowMachine_Nrpm` available in the Modelica package `Buildings.Fluid.Movers`. Any characteristic curve of axial fans with induction motors implicitly defines a function (i.e. a look-up table) that relates volume flow rate Q_{fan} and angular speed Ω_m to pressure drop $\Delta P_{fan} = \Delta P_{fan}(Q_{fan}, \Omega_m)$. Mechanical power P_m generated by the electric motor is partly converted to hydraulic work $W_{Flo} = \Delta P_{fan} \cdot Q_{fan}$ based on hydraulic efficiency η_{Hyd}:

$$P_m = \frac{W_{Flo}}{\eta_{Hyd}} = \frac{\Delta P_{fan} \cdot Q_{fan}}{\eta_{Hyd}} \tag{2}$$

where η_{Hyd} is also provided as a look-up table. The fan performance significantly depends on its hydraulic efficiency, and this parameter belongs to the group of parameters which were calibrated from measured data, as explained in sub-section 4.2. The rise in pressure generated by the axial fan was applied to two pipes that represent the inlet and outlet ventilation ducts.

The red connector between the motor and the impeller of the fan is used to connect the motor heat port and the impeller heat port, that physically takes into account that air is heated by the fan motor while passing through the fan. The air columns on the left-hand side take into account the action exercised by the height of the fan shaft. The component on the right-hand side represents a valve that physically prevents air flow when the fan is switched off.

The physics of the asynchronous induction machine AIM, which is the central part of the fan model in Figure 1, was implemented in a new class, that is a phasor representation of the asynchronous inductance motor, as presented and thoroughly discussed in Beaty and Kirtley (1998). An induction motor that is supplied by a three-phase symmetrical and balanced supply system with frequency f and line (phase to phase) voltage (RMS) equal to V was considered. In induction motors, several wire loops for each phase winding are placed in slots in the inner periphery of the stator. The three-phase

stator winding mutually displaced in space, by means of the three-phase currents mutually displaced in phase, produces a revolving magnetic field in the air gap inside the motor. The rotor has a structure similar to the stator: it accommodates the rotor winding and, when shorted, the induced electromotive forces move electrons through it and produce rotor currents. The interaction between the revolving magnetic field and the rotor currents produces motor torque and, thus, rotation.

If the motor has p pole pairs in the stator winding, then the synchronous speed is given by:

$$\omega_{sync} = \frac{\omega}{p} \tag{3}$$

where $\omega = 2\pi f$. The speed ω_R at which the magnetic field cuts the secondary conductors is equal to the difference between the synchronous speed and the real rotor speed ω_m:

$$\omega_R = \omega_{sync} - \omega_m \tag{4}$$

The ratio between the speed of the field related to the rotor and the synchronous speed is called the slip $s = \frac{\omega_R}{\omega_{sync}}$. If we define the speed of the rotating magnetic field with respect to the rotor:

$$\omega_s = \omega - p\omega_m \tag{5}$$

the slip can be redefined as:

$$s = \frac{\omega_s}{\omega} \tag{6}$$

whose meaning is of critical importance because s is the ratio between the power dissipated as rotor-circuit loss and the total power delivered to the motor. As a consequence, the remaining part $1 - s$ is the ratio that is converted into mechanical power. In order to model this phenomenon, the electrical model of the motor is expressed in a dq reference frame, according to Park's transformation, which is well described in Beaty and Kirtley (1998). As a result, the analytics of the model are simplified because the stator and rotor variables are referred to a reference frame that rotates with angular speed ω with respect to the stator. The angular speed ω is not bound to be constant.

The three-phase system is then transformed into an equivalent two-phase system. In this new frame the two axes are called the direct or d axis and the quadrature or q axis, respectively. The corresponding electrical quantities will be denoted with subscripts d and q, respectively. Finally, variables referred to the stator and rotor will be denoted with subscripts s and r, respectively. Hence, the machine dynamics are described by the following flux-current relationships referred to the stator:

$$\begin{bmatrix} \lambda_{dS} \\ \lambda_{dR} \end{bmatrix} = \begin{bmatrix} L_S & M \\ M & L_R \end{bmatrix} \begin{bmatrix} i_{dS} \\ i_{dR} \end{bmatrix} \tag{7}$$

and:

$$\begin{bmatrix} \lambda_{qS} \\ \lambda_{qR} \end{bmatrix} = \begin{bmatrix} L_S & M \\ M & L_R \end{bmatrix} \begin{bmatrix} i_{qS} \\ i_{qR} \end{bmatrix} \tag{8}$$

where λ is magnetic flux, i is electric current, M is stator-to-rotor mutual inductance, L_S and L_R are stator and rotor self-inductances that include stator and rotor leakage terms $L_S = M + L_{Sl}$ and $L_R = M + L_{Rl}$. The voltage equations are:

$$V_{dS} = \frac{d\lambda_{dS}}{dt} - \omega\lambda_{qS} + r_S i_{dS} \tag{9}$$

$$V_{qS} = \frac{d\lambda_{qS}}{dt} - \omega\lambda_{dS} + r_S i_{qS} \tag{10}$$

$$V_{dR} = \frac{d\lambda_{dR}}{dt} - \omega_s\lambda_{qR} + r_R i_{dR} \tag{11}$$

$$V_{qR} = \frac{d\lambda_{qR}}{dt} - \omega_s\lambda_{dR} + r_R i_{qR} \tag{12}$$

The developed torque can also be written as a combination of the aforementioned variables:

$$T_e = \frac{3}{2} p \left(\lambda_{dS} i_{qS} - \lambda_{qS} i_{dS}\right) \tag{13}$$

As already stated, the motor is assumed to be supplied by a balanced and symmetric three-phase system with effective (RMS) voltage V and effective current I. Single stator windings are supplied differently according to whether they are connected through either a star (Y) or a delta (Δ) connec-

tion. In the case of a star connection:

$$V = \sqrt{\frac{3}{2}}\sqrt{v_{dS}^2 + v_{qS}^2} \tag{14}$$

$$I = \sqrt{\frac{1}{2}}\sqrt{i_{dS}^2 + i_{qS}^2} \tag{15}$$

On the contrary, for a delta connection:

$$V = \sqrt{\frac{1}{2}}\sqrt{v_{dS}^2 + v_{qS}^2} \tag{16}$$

$$I = \sqrt{\frac{3}{2}}\sqrt{i_{dS}^2 + i_{qS}^2} \tag{17}$$

The equations listed above are numerous enough to capture the motor dynamics, provided that the following simplifying assumptions are met:

$$v_{qS} = v_{dR} = v_{qR} = 0 \tag{18}$$

the first of which states that the supply voltage is described by just the real part (i.e. its phase is null) and the last two equations meaning that the rotor is shorted (as usual).

At this stage, the performance and characteristics of the motor can be worked out. The rotational version of Newton's second law implies that the algebraic sum of the torque generated by the electric motor and the load torque T_m applied to the flange of a mechanical system (e.g. impeller) with

a moment of inertia J gives back an angular acceleration quantified as:

$$T_e - T_m = J\frac{d\omega_m}{dt} \tag{19}$$

The corresponding mechanical power P_m acting on the flange will be:

$$P_m = T_e\omega_m \tag{20}$$

The electric power absorbed by the induction motor will be made up of active (P) and reactive (Q) orthogonal components, which form a complex apparent power whose intensity is S and phase is Φ. Based on these definitions, the power factor will be $PF = \cos\Phi$ and the motor power will be derived as:

$$P = \sqrt{3}VI\cos\Phi \tag{21}$$

$$Q = \sqrt{3}VI\sin\Phi \tag{22}$$

$$S = \sqrt{P^2 + Q^2} \tag{23}$$

Motor efficiency η is computed as the mechanical to absorbed power ratio:

$$\eta = \frac{P_m}{P} \tag{24}$$

and the angular position of the flange θ is derived from the integral of the

mechanical speed:

$$\frac{d\theta}{dt} = \omega_m \tag{25}$$

All the equations reported in this sub-section were implemented in the component no. 7 of the DP-model depicted on Figure 1.

4. Calibration of the Modelica/Dymola model

4.1. The test-bed

The mechanical air supply system used as a test-bed is installed on Passeig de Gràcia line no. 3 (hereafter referred to as PdG-Line3). The metro station considered is located at the intersection of Carrer d'Aragó and Passeig de Gràcia avenues in Barcelona. The test-bed includes all the spaces that are typical of a metro station: commercial activities, technical rooms, public spaces open to passengers (i.e. accesses, transit zones, platforms) and staff only areas (e.g. offices, changing rooms, meeting rooms). The station layout consists mainly of low corridors, across which the air supply is partly provided by a mechanical air supply system and partly determined by wind pressure at the entrances and by the piston effect of trains. The metro service on working days starts at 5:00 am until midnight, except on Fridays when it is open until 2:00 am. On Saturday mornings, the station opens at 5:00 am and remains open throughout the night until midnight on Sundays. Mechanical ventilation is coordinated with the fans placed in the tunnels. The amount

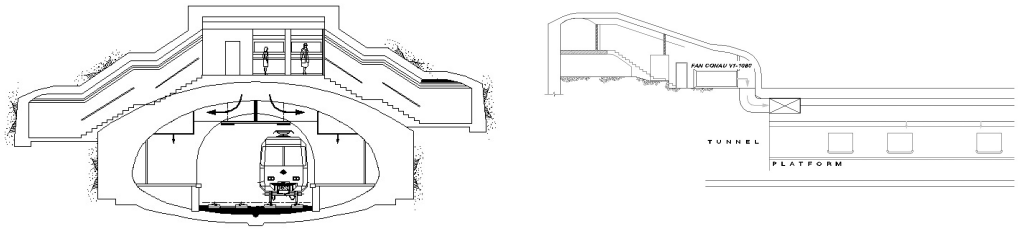

(a) (b)

Figure 2: Cross-section along the air path determined by the mechanical air supply system (a) and air intake above the platform in the PdG-Line3 (b).

of guaranteed air changes was sized on the basis of the maximum occupant density predicted in the station.

The mechanical air supply system in PdG-Line3 metro station (2) is responsible for limiting pollution (mainly measured by means of PM_{10} and CO_2 concentration in the air) and for setting air temperature at acceptable levels. The rate at which outdoor air is supplied, is differentiated according to the season and hour of the day. The functioning of the fans is regulated differently on the basis of daytime and nighttime. In summer time, when the station is open, design inward air flow pushed by the station fans amounts to about $60000m^3/h$ on each side of the platform. Design air flow rates extracted by each of the two fans in the tunnels is about $Q_2 = 90000m^3/h$. These conditions should generate a design net air flow per fan through corridors and passageways amounting to about $Q_3 = 30000m^3/h$, whose real value is of course subject to variations, determined by outdoor weather, internal temperature dynamics, number of passengers, trains and other disturbances.

In summer all the fans are driven at their maximum rotational speed,

while in the winter they are driven at half their maximum rotational speed. Such a predetermined schedule causes energy waste whenever those air flow rates are not strictly required to maintain acceptable comfort conditions in the station. Therefore, this is one of the typical cases where active control through VFD devices can improve the functioning of fans according to real needs and, as a result, would reduce the overall energy consumption in the station.

The modeling effort that is reported in this paper concerned the two injecting fans placed in the station, that work in parallel in a technical room, where they direct the outdoor air onto the platform, following the path represented by the cross-section in Figure 2-a. The air intake is located in the fan room ceiling at road level; the fans in the room provide increase in pressure which is needed to push air across the distribution system. In order to distribute ventilation air properly, outdoor air is finally delivered by thirteen vents on each side of the plenum above the platform, indicated by the line in Figure 2-b. Each fan is of the CONAU V11080 type that is run by a 15 kW electric induction motor at 1500 rpm at no load. It should be noticed that the working point expected for this application falls around a volume flow equal to $62500 m^3/h$ and a static pressure of $35 mm H_2 0$, equivalent to 343 Pa. This generates at most $15 kW$ power consumption obtained thanks to a blade pitch of approximately $35° - 40°$, which is not dynamically adjustable. Table 1 shows the main technical features of the fans and their three-phase current induction motors. The blade rotational speed of the fans can be adjusted by

Codes of fans	VE 3-27-2 / VE 3-27-3
Manufacturer - Model	CONAU ASEA - V1/1080
Motor Power	$18.5CV$
Supply voltage	3 x $230V$
Maximum Power	$15kW$
Number of poles	4
Rpm	$1500min^{-1}$
Nominal current	$29A$
Load factor	0.85
Nominal airflow rate	$62500m^3/h$
Nominal static pressure	$35mmH_2O$
Blade pitch	$35° - 40°$
Reversible	yes
VFD	yes
Grate size	1.6m by 5m

Table 1: Main features of the fans and the corresponding electric motors.

means of a Variable Frequency Drive (VFD). This device is currently used to halve the speed in winter, in order to control the two fan induction motors in their starting phase. In fact, when an induction motor is simply connected to the electrical grid (i.e. across-the-line starting), since its *slip* is very large, the starting current is very high: in the order of five to six times the rated full-load current (Ref. Beaty and Kirtley (1998)). This may also cause a significant voltage drop which, as a result, may affect other customers connected to the same electrical grid. Thanks to VFDs, starting currents are made less intense and gentler, despite the fact that a certain dynamics are still present. Hence, not all its potential is currently exploited and VFD can be programmed in order to adjust the fan rates to real ventilation needs.

4.2. Calibration and validation with measured data

A trial was performed on site in order to set up an experimental benchmark. Figure 3-a shows the active power absorbed by the fan while input frequencies are varied from 0 Hz (1st step) through 25 Hz (2nd step) up to 50 Hz (3rd step). So, the fans were driven first at half their speed (i.e. 25 Hz) and then at their full speed (i.e. 50 Hz). According to the affinity laws of fans, rotational speed varies linearly with the air flow rate of fans. As a consequence, even the air flow rate of the fans varied between half their full capacity and their full capacity. In this range the total efficiency of the fans is affected by their hydraulic efficiency only, while the motor and converter efficiency are almost constant, as reported by Markusson (2011). Therefore, this part of the calibration was based on that parameter, whose value depends on the rated volume (i.e. the ratio between the real air flow rate and the maximum air flow rate).

In order to determine the best fitting hydraulic efficiency plot, several numerical simulations were carried out. Considering that the fan frequencies during the tests were known and that real hydraulic efficiency is dependent on the air flow rate of the fans, the best fitting values of hydraulic efficiency were surveyed separately for the winter and summer modes. As a result, it was possible to calculate the values in Table 2, which show that eta = 0.50 is the best value in the low rate case, while eta = 0.82 is the best value in the high rate case, because they generate the lowest differences between the reference and the simulated active power. Some of the other tested values

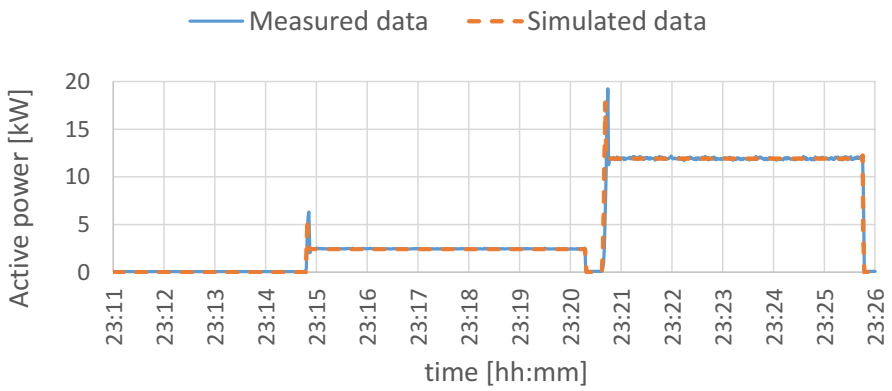

(a)

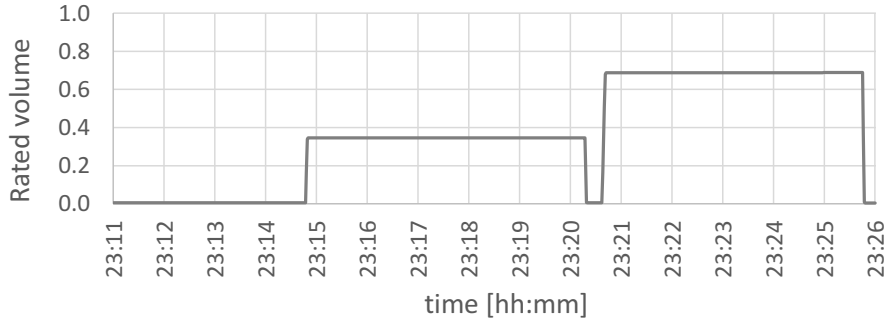

(b)

Figure 3: Active power plot of the fan tested under transient conditions (a) and simulation of the rated volume provided by the fans when running at low and high frequency (b).

	Active power (kW)			
	Fan frequency = $25Hz$		Fan frequency = $50Hz$	
η	Reference	Simulated	Reference	Simulated
0.50	2.45	2.459	11.94	19.16
0.51	2.45	2.382	11.94	18.575
0.55	2.45	2.241	11.94	17.47
0.60	2.45	2.059	11.94	16.06
0.65	2.45	1.90	11.94	14.86
0.70	2.45	1.77	11.94	13.83
0.75	2.45	1.65	11.94	12.39
0.80	2.45	1.55	11.94	12.14
0.82	2.45	1.509	11.94	11.77
0.85	2.45	1.46	11.94	11.4

Table 2: Power absorbed by the fan computed at several fan frequency values.

for η (spaced at a 0.5 Hz frequency step) were included in the table in order to provide a description of the variation in fan power according to the value of hydraulic efficiency.

The best curve for η was also included as an input in the model *Impeller* component, by plotting a curve interpolating the two points defined by the rated volume (r_V) depicted in Figure 3-b and the corresponding efficiency values. The rated volume at which the fans work in the two operational modes is dependent on the functioning points of the fan, when they are subject to the pressure load caused by piping and by the station. Therefore, these points were worked out by means of a simulation of the whole PdG Dymola model and, as shown in Figure 3-b, they are equal to, respectively, $r_V = 0.345$ when the fans are driven at 25 Hz, and $r_V = 0.688$ when the fans are driven at 50 Hz. Hence, the final input assigned to the field `HydrEta` of the class `Fan.AIM` in the PdG Dymola model was: $r_V = 0.345, 0.688$ and

$\eta = 0.50, 0.82$. Figure 3 shows that the curve interpolated by the software between these two points accurately matches the energy power absorbed by the fans when they are operated at 25 and 50 Hz. Furthermore, the empirical hydraulic efficiency values obtained from experimental measurements are in good agreement with the plots regarding "relative flow rate" vs "hydraulic efficiency" provided in Markusson (2011) for the case of pumps and fans installed in systems with constant pressure values. Hence the technical information reported in that publication would suggest using similar inputs to the model.

The second step of the calibration process concerned the electronic parameters of the fan model described in sub-section 3.2, namely the stator and rotor resistances (R_s and R_r), the mutual inductance (M), the stator and rotor self-inductances (L_s and L_r), the impeller moment of inertia (J). In addition, the inverter schedule was also checked. In other words, the *inverter* component shown in Figure 1 includes the schedule at which the fan impeller was driven during the test, when the fan was manually activated first up to 25 Hz and then up to 50 Hz. Initially, an activation time as long as $2s$ was assumed for both the first and second starting operations of the fan, but, as will be shown later, the simulation and the tests match better if the second starting time is slightly increased.

As a first attempt, the electronic parameters were set according to the suggestions made by some authors who had already performed estimations regarding similar induction motors (ref. Kral et al. (2009)). A number of

further simulations were then carried out in order to match experimental results with those deriving from the simulations by means of electrical parameter adjustment. As far as electrical parameters are concerned, Pedra (2006) showed that self-inductances are those which mostly affect the shape and intensity of peak power values. Hence, these parameters were varied within a certain range around the initial values, until the curve shape resembled the one that was experimentally measured. Peak intensity also proved to be strongly influenced by the impeller moment of inertia, whose variation had a significant impact on the accuracy of the simulated plots with respect to the measured plot. Table 3 lists some of the results from the simulations.

It can be noticed that the 7^{th} case, whose final curve is shown in Figure 3-a (labeled as "simulated data"), is the one which gave back the best match. Scientific assessment of the quality of simulations was performed in terms of comparison between the measured active power absorbed by one of the two fans during its dynamic activation and the simulated power. As the recording step was 1 s and measurements were taken from 11:11 pm to 11:26 pm, a time series of 901 records was finally available. The modeling deviation was estimated by means of two indicators suggested by reference standards. Mean Bias Error (MBE) and Cumulative Variation of Root Mean Square Error (CVRMSE) values were calculated using the formulae suggested by Committee et al. (2002), which have been already applied both for the validation of energy models against hourly measurements (Raftery et al. (2011)) and for the calibration of transient models based on Modelica/Dymola (Ali

ID	L_s	L_r	M	R_r	R_s	J	t_{rise}	MBE %	$CVRMSE$ %
1	0.008	0.008	0.268	0.563	0.478	2	2	-0.53	28.81
2	0.020	0.020	0.268	0.563	0.478	2	2	58.56	99.94
3	0.013	0.013	0.268	0.563	0.478	2	2	0.13	14.58
4	0.011	0.011	0.268	0.563	0.478	2	2	0.54	20.48
5	0.011	0.011	0.268	0.563	0.478	1	2	0.20	19.71
6	0.011	0.011	0.268	0.563	0.478	2	4	0.02	17.85
7	0.011	0.011	0.268	0.563	0.478	1	4	0.66	12.57
8	0.011	0.011	0.268	0.563	0.478	1.5	4	0.35	14.91
9	0.011	0.011	0.268	0.563	0.478	1.25	4	0.50	13.78
10	0.011	0.011	0.268	0.563	0.478	1.15	4	0.56	13.40

Table 3: Simulation results for different parameters setup for calibrating the DP fan model. Percent values of MBE and CVRMSE are reported for each testing combination.

et al. (2015)):

$$MBE = \frac{\sum_{i=1}^{N_P}(M_i - S_i)}{\sum_{i=1}^{N_P} M_i} \tag{26}$$

$$CVRMSE = \frac{\sqrt{\frac{1}{N_P}\sum_{i=1}^{N_P}(M_i - S_i)^2}}{\frac{1}{N_P}\sum_{i=1}^{N_P} M_i} \tag{27}$$

where M_i is the list of measured data, S_i is the set of simulated data and N_P is the size of the database.

MBE and CVRMSE are used to validate simulation models. The finest simulation step and time step for recording measurements considered by the reference technical standard is 1 minute (Standard 55-1981 ed. Tech. rep. and Engineers (2004)), to which maximum admissible percentage errors equal to 10% and 30% correspond, respectively. Lower thresholds are set in case the time step is coarser; instead the finer the time step the higher the admissible

error can be. As a consequence, considering that the simulation time step and the measurement time step in our case was equal to 1 s, but the finest time step considered by the technical reference standard is 1 min, a model whose MBE and CVRMSE are lower than 10% and 30% must be a good one. This is the case for almost all the simulations reported in Table 3, among which the 7^{th} simulation case appears to be the best overall, hence the parameters belonging to case no. 7 were set as the ones to be used for the models adopted in the comparative study presented in section 5. The validation was considered successful because the calibrated model presented $MBE = 0.66\% < 10\%$ and $CVRMSE = 12.57\% < 30\%$.

5. Comparison with other Modelica/Dymola models

5.1. The other models used for comparison

The phasor representation model (DP-model) described in sub-section 4 was compared with two other models, that are based on two opposite concepts:

- the basic stationary model (*S-model*), that is not able to simulate the whole dynamics of a fan, and that was mainly based on the `Flow_machine_Nrpm` component of the `Modelica.Buildings` library;
- the dynamic time domain model (*DT-model*), that is based on the `AIM_squirrel_cage` component of the `Modelica.Buildings` library.

With respect to the structure described in sub-section 4 about the DP-model, the aforementioned two models differ in components (6), (7) and (8), that is the impeller, the electric motor and the inverter, respectively (please ref. to Fig. 1).

In the S-model (Figure 4-a), the impeller (6) and the electric motor (7) are both modeled by using two identical instances of the `FlowMachine_Nrpm` object from the `Buildings.Fluid.Movers` package, connected in opposite directions and slightly adjusted in order to also allow for reverse flow when the motor is turned-off. The inverter (8) implements a proportional relation between input frequency (Hz) and revolutions per minute (RPM) and applies the latter to the corresponding fan, depending on the sign of the input frequency. Therefore, in the S-model, both the electric motor and the impeller are modeled with their stationary characteristic curves. In order to implement the dynamics of the electric motor, the impeller model has been extracted from the `Buildings` library and is represented in the DT-model and DP-model as component (6).

In the DT-model (Figure 4-b), all the time domain dynamics of the asynchronous induction motor are implemented using one instance of the `AIM_SquirrelCage` object from the `Modelica.Electrical.Machines` package. The terminal box of the motor, the inverter and the power sensor has been taken from the `Modelica.Electrical.Machines` package. The electrical three-phase voltage source was also taken from the `Modelica.Electrical.MultiPhase` package.

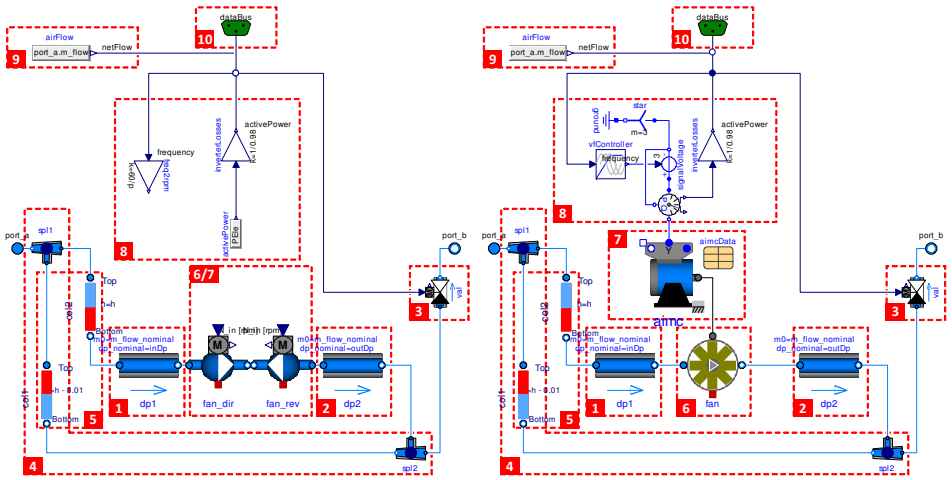

Figure 4: The graphic representations in Dymola of the basic stationary model (a) and of the time domain model (b): (1)/(2) inlet/outlet fan ducts, (3) valve, (4) leakage, (5) air columns, (6) axial impeller, (7) electric motor, (8) inverter, (9) air flow sensor, (10) I/O data bus.

As a result, the physics of the S-model and DT-model are derived from known libraries offered by Modelica. On the contrary, the physics of the DP-model is not available in any other library, yet.

5.2. Performance comparison for power consumption prediction

In order to compare the performances of the three models, in terms of accuracy to predict the dynamic behavior of fans, the detailed DT-model was assumed as the reference one, and deviations provided by the S-model and DP-model from the first one were estimated. To this purpose, two different studies were conducted for the three models using the same parameters listed in Table 4.

The first study is based on the evidence that, since a general fan input

Parameter	Description	Value
col1.h, col2.h	Height of ventilation shaft	$0m$
dp1.m_flow_nominal= dp2.m_flow_nominal= val.m_flow_nominal	Nominal mass flow rate	$20kg/s$
dp1.dp_nominal	Inlet pressure drop at nominal flow rate	$20Pa$
dp2.dp_nominal	Outlet pressure drop at nominal flow rate	$500Pa$
val.dpValve_nominal	Nominal pressure drop of fully open valve	$1Pa$
val.dpFixed_nominal	Pressure drop of pipe and other resistances that are in series	$1Pa$
val.l	Valve leakage	0.001
spl1.m_flow_nominal= spl2.m_flow_nominal		$\{20, 20, 20\}kg/s$
spl1.dp_nominal		$\{1, 1, 1\}Pa$
spl2.dp_nominal		$\{3.3, 100, 3.3\}Pa$
fan.hydraulicEffciency.r_V	Normalized volume flow rate	$\{0.345, 0.688\}$
fan.hydraulicEffciency.eta	Efficiency at given normalized volume flow rate	$\{0.50, 0.82\}$
fan.N_nominal	Nominal rotational speed for flow characteristics	$1470min^{-1}$
fan.pressure.V_flow	Volume flow rate at user-selected operating points	$\{10, 12, 14, 16, 18, 20\}m^3/s$
fan.pressure.dp	Fan total pressure at user-selected operating points	$\{860, 800, 700, 565, 410, 250\}Pa$
inverter.invEfficiency	Efficiency of the inverter	98%
inverter .nominalFrequency	Nominal frequency	$50Hz$
inverter.nominalVoltage	Nominal voltage at nominal frequency	$380V$
AIM.J=aimcData.Jr	Rotor moment of inertia (including load)	$1.2kgm^2$
AIM.p=aimcData.p	Number of pole pairs	2
AIM.Rs=aimcData.Rs	Stator resistance per phase	0.478Ω
AIM.Rr=aimcData.Rr	Rotor resistance (equivalent three-phase winding)	0.563Ω
AIM.Lsl=AIM.Lrl= aimcData.Lssigma= aimcData.Lrsigma	Stator and rotor stray inductance per phase	$0.008H$
AIM.M=aimcData.Lm	Main field inductance	$0.268H$

Table 4: Main parameters of the three fan models used for comparing performance and computational burden.

can be represented as a series of sines and cosines (as stated by the Fourier's theory), a frequency analysis of the outcomes of the three fan models can be performed and the results can be analyzed as a frequency response chart. It is then assumed that the input power supplied to the fan has a frequency f that varies with time as $f(t) = \frac{f^{max}}{2}(1 + \sin(2\pi F t))$. The relevance of this first study is motivated by the opportunity of finding out the frequency ranges beyond which the behavior of the fans differentiate. This suggests which dynamics the S-model and DP-model are able to catch, with respect to the top performing DT-model. On the contrary, the purpose of the second study is to evaluate how big the deviation in terms of power consumption between the three fans is, in case they are simulated over a whole day of operation.

To this purpose, a power RMSE index $e_{P\%}$ is defined as the root mean square error of the absorbed active power P_i of a model w.r.t. that one of the DT-model P_i^{DT}, calculated as the percentage of mean power of the latter:

$$\text{Power RMSE} \doteq e_{P\%} \doteq 100 \frac{\sqrt{\frac{1}{n}\sum_{i=1}^{n}(P_i - P_i^{DT})^2}}{\frac{1}{n}\sum_{i=1}^{n} P_i^{DT}} \tag{28}$$

The total energy error $e_{E\%}$ is computed as the percentage difference of the energy for the considered model E and that one for the DT-model E^{DT}:

$$\text{Final energy error} \doteq e_{E\%} \doteq 100 \frac{E - E^{DT}}{E^{DT}} \tag{29}$$

A speedup factor is then defined to indicate how many times faster the simulation is w.r.t. the DT-model.

Figures 5 and 6 show the corresponding simulation results achieved with Dymola 2016 running on a machine with CPU Intel® Core^{TM} i7 CPU Q720@1.60GHz, RAM 8GB, OS Windows 7@64bit. The simulation step was set to 0.01s and solver type Sdirk34hw with tolerance 10^{-5} over a simulation interval equal to [0; 960s]. Figures 5-a and 5-b show that, w.r.t. the reference DT-model, the DP-model is 2-10 times faster and the S-model is 5-10 times faster. Below the frequency of 200mHz, the two computational times for the DP-model and the S-model almost converge. Regarding the accuracy, the DP-model has always a negligible error w.r.t. the reference DT-model, whereas the S-model always shows significant power errors and sensible energy error for $F > 10mHz$. The DP-model produces the largest error (at the most 7% for power and about 0.5% for energy) at high frequencies F. This happens because, when the frequency increases, the assumption of a sinusoidal regime begins to lose its validity and the phasor representation starts to show its limits.

Time constants of controllable thermal dynamics of building are in general greater than $600s$ and an air temperature sensor has typical time constants in the order of $1min$, that corresponds to a bandwidth $f_{-3dB} = 1/(2\pi\tau) = 2.65mHz$. Thus, the control frequency F_c, that is the rate at which the control input is updated, can be reasonably upper limited by $F_c \leq 2mHz$. The fan is then driven by an input whose fundamental frequency is half the

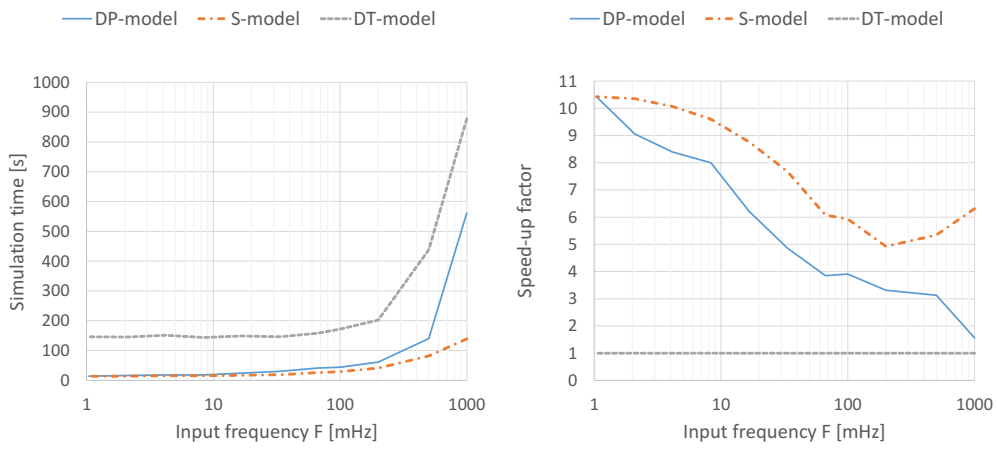

(a) (b)

Figure 5: Comparison between the three developed models in terms of simulation time (a) and speed up factors (b).

control frequency and, considering that harmonics amplitude progressively decrease, the main harmonic content is typically included between $1mHz$ and $100mHz$, where the DP-model shows its best performance. The total energy estimation is very accurate in the whole range, since its accuracy is in the order of 0.5% and the DP-model can be used without losing dynamic information but with an important speed-up factor w.r.t. the DT-model (from 7 to 10 times faster in the considered range).

Anyway, in order to gain a better understanding about the accuracy in energy estimation by the three models, they were run over a typical one-day operation, that was obtained from whole building operation of the station described in sub-section 4.1, as better explained in the contribution by Vaccarini et al. (2016). So, the fan frequency shown in Figure 7 was used as

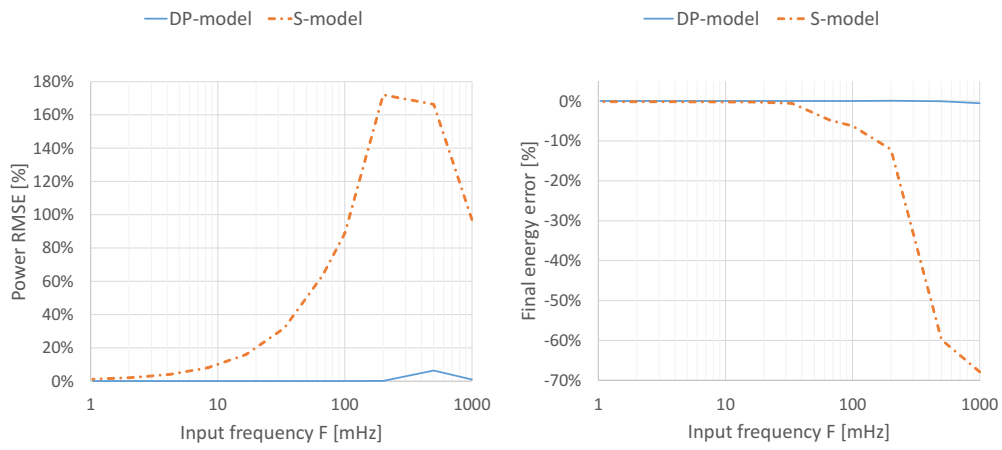

(a) (b)

Figure 6: Comparison between the three developed models in terms of power RMSE (a) and energy error (b).

the same input to the three fan models. Then, the power consumption estimated by the three fans, were compared. As in confirmed by the plots in Figure 7, it came out that if the DT-model is chosen as the benchmark and top performing model, the Power RMSE (root mean square value) referred to the mean absorbed power for the DT-model is equal to $e^{S}_{P\%} = 0.34\%$ for the S-model and to $e^{DP}_{P\%} = 0.02\%$ for the DP-model. These power errors corresponds to a final energy error equal to $e^{S}_{E\%} = 0.27\%$ for the S-model and to $e^{DP}_{E\%} = 0.02\%$ for the DP-model. It can also be noticed from the power error plot of Figure 7 that, but the model biases, the main dynamic mismatch occur for the S-model when the fan frequency input varies more rapidly, whereas the DP-model still matches the reference.

In order to consider more general situations in which the controller acts

more dynamically than in the subway station (where $F_c = 600s$), other tests were performed using a white noise as frequency input to the fans. In these conditions the DP-model showed substantially unchanged performance both in term of power and energy errors. With unchanged control interval, the power RMSE increased to $e^S_{P\%} = 4.46\%$ and the final energy error increased to $e^S_{E\%} = 1.07\%$. Decreasing the control interval to $F_c = 60s$, the white noise input produced a power RMSE up to $e^S_{P\%} = 8.58\%$ and a final energy error equal to $e^S_{E\%} = 2.94\%$.

So, it was shown that the performance, in terms of power consumption estimation, offered by the DP-model is much better than what can be offered by the S-model and is quite close to the output of the DT-model, in particular when rapidly varying control inputs are applied. Moreover the computational burden required by the DP-model is a good trade-off between the S-model and the DT-model.

6. Conclusions

The calibrated DP-model, which is based on the phasor representation, was shown to be able to simulate experimental data with deviations well below the thresholds set by related technical standards. When the DP-model was compared with the top performing DT-model, it was shown to be between 2 and 10 times faster, while presenting negligible deviations in terms of estimated power consumption, within the control frequency range that can reasonably occur in ventilation systems driven by VFDs. This

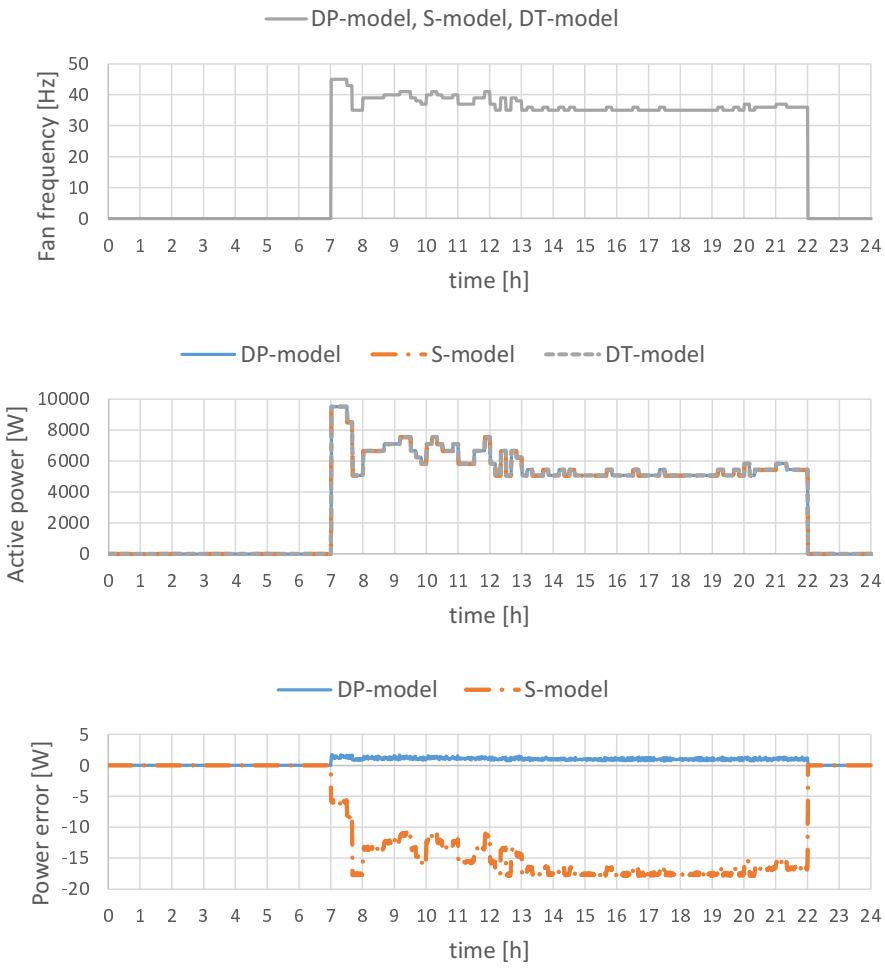

Figure 7: Plot of the frequency input provided to the three fans and their corresponding estimation of active power consumption and power error with respect to the reference DT-model.

result is confirmed by the one day long simulation over a typical day when the fan was controlled dynamically by a VFD: the deviation of the energy consumption estimated by the S-model was more than ten times higher than the one associated to the DP-model (i.e. 0.27% and 0.02%, respectively). Also, it was shown that the more dinamically was the fan driven, the higher that deviation difference becomes.

For the reasons stated above, the DP-model for transient simulation of induction motor fans was both accurate and efficient in terms of computational burden, that makes it suitable for integration in complex simulation domains in the fields of building design and control.

7. Acknowledgments

The authors are greatly indebted to Eng. Valerio Costantini and TMB staff, for their support during the on-site measurements.

The work presented in this paper was co-funded by the European Commission within the Seam4us project (contract no. 285408).

8. References

Aghemo, C., Blaso, L., Pellegrino, A., 2014. Building automation and control systems: A case study to evaluate the energy and environmental performances of a lighting control system in offices. Automation in Construction 43, 10–22.

Ali, M., Vukovic, V., Sahir, M. H., Fontanella, G., 2013. Energy analysis of chilled water system configurations using simulation-based optimization. Energy and Buildings 59, 111–122.

Ali, M., Vukovic, V., Sheikh, N. A., Ali, H. M., Sahir, M. H., 2015. Enhancement and integration of desiccant evaporative cooling system model calibrated and validated under transient operating conditions. Applied Thermal Engineering 75, 1093–1105.

Beaty, H. W., Kirtley, J. L., 1998. Electric motor handbook. McGraw-Hill Professional.

Canelli, M., Entchev, E., Sasso, M., Yang, L., Ghorab, M., 2015. Dynamic simulations of hybrid energy systems in load sharing application. Applied Thermal Engineering 78, 315–325.

Cellier, F. E., Kofman, E., 2006. Continuous system simulation. Springer Science & Business Media.

Chen, Y., Treado, S., 2014. Development of a simulation platform based on dynamic models for hvac control analysis. Energy and Buildings 68, 376–386.

Committee, A. S., et al., 2002. Ashrae guideline 14-2002 measurement of energy and demand savings.

Ferkl, L., Meinsma, G., 2007. Finding optimal ventilation control for highway tunnels. Tunnelling and underground space technology 22 (2), 222–229.

Ha, Q., Vakiloroaya, V., 2015. Modeling and optimal control of an energy-efficient hybrid solar air conditioning system. Automation in Construction 49, 262–270.

Kral, C., Haumer, A., Grabner, C., 2009. Consistent induction motor parameters for the calculation of partial load efficiencies. In: Proceedings of the World Congress on Engineering. Vol. 1. pp. 1–3.

Li, P., Li, Y., Seem, J. E., 2009. Modelica based dynamic modeling of an air-side economizer. In: ASME 2009 International Mechanical Engineering Congress and Exposition. American Society of Mechanical Engineers, pp. 811–820.

Li, Y., Liu, M., Lau, J., 2015. Development of a variable speed compressor power model for single-stage packaged dx rooftop units. Applied Thermal Engineering 78, 110–117.

Markusson, C., 2011. Efficiency of building related pump and fan operation-Application and system solutions. Chalmers University of Technology.

Nagano, K., Katsura, T., Takeda, S., 2006. Development of a design and performance prediction tool for the ground source heat pump system. Applied Thermal Engineering 26 (14), 1578–1592.

Park, B., Krarti, M., 2015. Development of a simulation analysis environment for ventilated slab systems. Applied Thermal Engineering 87, 66–78.

Pedra, J., 2006. Estimation of typical squirrel-cage induction motor parameters for dynamic performance simulation. IEE Proceedings-Generation, Transmission and Distribution 153 (2), 137–146.

Raftery, P., Keane, M., Costa, A., 2011. Calibrating whole building energy models: Detailed case study using hourly measured data. Energy and Buildings 43 (12), 3666–3679.

Standard 55-1981 ed. Tech. rep., Standard 55-1981 ed. Tech. rep. American Society of Heating, R., Engineers, A. C., April 2004. Thermal environmental conditions for human occupancy. ASHRAE.

Starkloff, R., Alobaid, F., Karner, K., Epple, B., Schmitz, M., Boehm, F., 2015. Development and validation of a dynamic simulation model for a large coal-fired power plant. Applied Thermal Engineering 91, 496–506.

Tomažič, S., Logar, V., Kristl, Ž., Krainer, A., Škrjanc, I., Košir, M., 2013. Indoor-environment simulator for control design purposes. Building and environment 70, 60–72.

Traore, I., Gavan, V., Riffonneau, Y., L'Henoret, B., Drouet, E., 2013. Development of a generic and scalable modelica based model of a typical french railway station building. IBPSA 13, 2139–2146.

Trčka, M., Hensen, J. L., 2010. Overview of hvac system simulation. Automation in Construction 19 (2), 93–99.

Vaccarini, M., Giretti, A., Tolve, L., Casals, M., 2016. Model predictive energy control of ventilation for underground stations. Energy and Buildings.

Wang, L., Wong, N. H., 2008. Coupled simulations for naturally ventilated residential buildings. Automation in Construction 17 (4), 386–398.

Wetter, M., 2009a. Modelica-based modelling and simulation to support research and development in building energy and control systems. Journal of Building Performance Simulation 2 (2), 143–161.

Wetter, M., 2009b. Modelica library for building heating, ventilation and air-conditioning systems. 7th Modelica Conference, Como, Italy, Sep. 20-22 1, 393–402.

Wetter, M., 2011. A view on future building system modeling and simulation. In: Jan L.M. Hensen and Roberto Lamberts "Building Performance Simulation for Design and Operation", Routledge, UK, Ch. 1, pp. 1–28, iSBN: 978-0-415-47414-6.

Wildi, T., 2002. Electrical machines, drives, and power systems.